Available online at www.sciencedirect.com

ScienceDirect

materialstoday: PROCEEDINGS

Materials Today: Proceedings 1S (2014) 122 – 129

Living Light: Uniting biology and photonics – A memorial meeting in honour of Prof Jean-Pol Vigneron

Nanostructured surfaces: bioinspiration for transparency, coloration and wettability

O. Deparis*, S. Mouchet, L. Dellieu, J.-F. Colomer, M. Sarrazin

Solid-state Physics Laboratory, Dept. of Physics, University of Namur, 61 rue de Bruxelles, Namur, B-5000, Belgium

Abstract

Natural nanostructures rarely come with a single biological function to fulfil. Moreover, from a bio-inspiration perspective, it sounds attractive to develop multifunctional coatings, devices or sensors. Suppression of light reflection from body parts, such as the wings of insects, is useful for hiding from predators. The transparent parts of the wings of *Cacostatia ossa* (moth) inherit their antireflective property from non-close-packed nano-scale nipple arrays on both sides of the wings. Through modelling and optical simulations, we show that effective medium approaches, commonly used to characterize antireflection, slightly overestimate the reflectance with respect to detailed Rigorous Coupled Wave Analysis calculation. Coloration due to light interference in nanostructure, on the other hand, sometimes comes with an additional, unexpected and maybe non-biologically significant function: hygrochromism, i.e. change of color with humidity. The male *Hoplia coerulea* (beetle), for instance, exhibits iridescent blue-violet color which turns to emerald green when the elytron is put in contact with water. Impregnation experiments with various liquids revealed intriguing color change dynamics which could be related to the wetting properties of porous chitinous cuticle. Super-hydrophobicity is another function of biological significance, which helps, for instance, insects to keep dry in humid environments. Through morphological, optical and contact angle measurements, we show the existence of entangled levels of functionality on the wings of *Cicada orni*, namely a superhydrophobic stage at the upper part of the nipple array corrugated surface and an antireflective stage and the lower part.

Selection and Peer-review under responsibility of Physics Department, University of Namur.

Keywords: Structural colors, antireflection coatings, hydrophobicity, optical sensors

* Corresponding author. Tel.: +32 81 725235; fax: +32 81 724464.
E-mail address: olivier.deparis@unamur.be

Selection and Peer-review under responsibility of Physics Department, University of Namur.
doi:10.1016/j.matpr.2014.09.008

1. Introduction

Natural photonic structures, such as surface corrugations or multilayers, rarely come with a single biological function to fulfil. For instance, nanostructures on the surface of cicada wings are responsible for super-hydrophobicity and self-cleaning [1], which helps the insect to stay dry and uncontaminated and hence ensures an important biological function. Another relevant biological function which is performed by the same nanostructure is related to camouflage. Indeed, the above mentioned surface corrugation acts also as an antireflection coating [2], which makes the wing "invisible" (i.e. perfectly transparent to light) and helps the insect to avoid being seen by predators. There are in nature interesting examples of physical properties, mainly structural colors, which change according to the environment. For instance, the greenish color of the tropical beetle *Dynastes hercules*, which arises from light interference within a porous multilayer in the beetle cuticle, turns to black upon exposure to humidity (RH>80%) [3]. The biological function, which is related to this hygrochromic property in *Dynastes hercules*, has not found definite explanation so far; hypotheses of camouflage or thermoregulation functions both conflict with other biological facts [3]. Nevertheless, the physical mechanism by which the reflectance of the beetle cuticle is tuned by flooding the porous multilayer with liquid has been quite well elucidated [3]. In a biomimetic approach, humidity thin-film sensors have been fabricated by replication of the beetle spongy multilayer using colloidal templating method and hydrophilic surface treatment [4]. Some beetles are also known to change their coloration reversibly in an active manner, upon an external stimulus (e.g. when they get stressed). For instance, the cuticle of the tortoise beetle *Charidotella egregia* turns to gold mirror color (due to a multilayer stack) to transparency (through refractive index homogenization) upon stress (likely by releasing physiological liquid in the multilayer) [5]. This color-to-transparency switching of a biological multilayer has inspired recently the fabrication of hygrochromic mesoporous dielectric multilayer coatings [6]. A rationale for the design of coatings that are switchable from transparency to highly saturated (Bragg) color upon infiltration of liquid in porous multilayer has been theoretically proposed [7]. Much has still to be discovered regarding the interplay of physical properties of natural nanostructures and their use for various biological functions. From a bio-inspiration perspective, it is attractive to develop multifunctional surfaces and coatings that combine, e.g., transparency and hydrophobicity (self-cleaning solar cell panels), coloration and wettability (optical sensors), etc.

In this article, the properties of transparency, structural coloration, and wettability are investigated in various natural nanostructures with the emphasis on the interplay between these properties that may have led to a biological advantage in the evolution of the related species and/or that are worth to be implemented in biomimetic materials and devices. Transparency is first studied in the exemplary case of *Cacostatia ossa* moth whose transparent wing parts inherit their antireflective property from non-close-packed nipple arrays on both sides of the wing [8]. Next, in connection with the above mentioned hygrochromic property, color changes in the *Hoplia coerulea* beetle upon contact with various liquids are studied [9]. During impregnation experiments with water and ethanol, counter-intuitive color changes are observed with respect to the expected affinities of bulk chitin with those liquids. A tentative explanation is put forward. Finally, wettability and transparency are studied in *Cicada orni*, where entangled levels of functionality are evidenced and confirmed by experiments and simulations; namely a superhydrophobic stage in the upper part of the nanostructure and an antireflective stage in the lower part [10].

2. Transparency

Close-packed nipple arrays are found on facet lenses of e.g. butterfly compound eyes, where they are organized in domains of hexagonal packing and provide efficient antireflection (AR) property [11]. Typical nipple inter-distances range from 180 to 240 nm and, since the protuberance sizes and inter-distances are shorter than visible light wavelengths, these nipple arrays act as effective graded-index AR layers [11].

Non-close-packed nipple arrays, with a lesser degree of order, were found on the transparent parts of the wings of *Cacostatia ossa* moth [8]. Nipple arrays were present on both sides of the wing, the thickness of the bulky membrane (*d*) being equal to about 1 µm (Fig. 1-a). A photonic model of the corrugated wing was devised based on morphological data from scanning electron microscopy (SEM) images (Fig. 1-b). Nipples were assimilated to

truncated cones with average top (bottom) radius equal to r=50 nm (R=120 nm) and average height equal to H=400nm. Due to the disorder and to the sub-wavelength size of the corrugation, the choice of the array type was not critical. A square array was used here with an average period equal to a=380 nm (for comparison, a hexagonal array was also tested and led to similar results [8]). Lateral periodicity of the wing surface corrugation is of the order of the wavelength of blue light, which implies that diffraction can only take place in the ultraviolet (UV) range. In comparison, the thickness of the wing membrane is much larger but it is still lower than sunlight coherence length, which implies that light interference (Fabry-Perot fringes) should be observed in the whole UV-visible-near infrared range. In particular, the influence of the back side corrugation cannot be discarded [8].

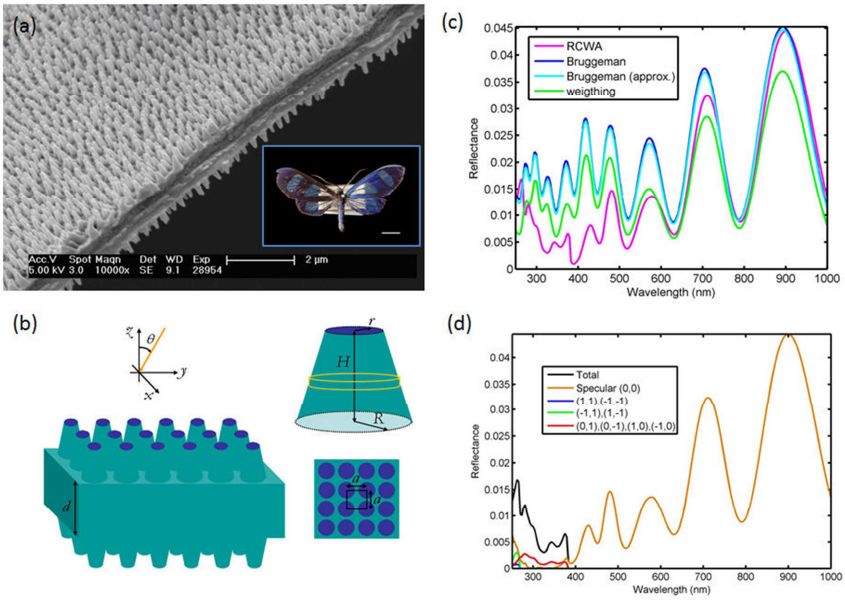

Fig. 1. (a) Scanning electron microscopy image of a transparent region of *Cacostatia ossa* (moth) wing where nipple array corrugation can be seen on both sides (inset: photograph of the specimen) [8]; (b) photonic model of the wing (d: membrane thickness, H, R, r: height and (upper/lower) radii of a nipple protuberance approximated by a truncated cone, a: spatial period of the nipple square array) [8]; (c) Reflectance spectrum of the wing model calculated by Rigorous Coupled wave Analysis (RCWA) and various effective medium methods [8]. (d) Contributions of diffraction orders ($\boldsymbol{g}(m,n)$: reciprocal lattice vector) and specular direction ($\boldsymbol{g}$=(0,0)) to the hemispherical (total) reflectance.

In order to isolate the effects of the photonic structure from those of the material dispersion, the extinction coefficient of the material (chitin) was taken constant across the whole spectral range: n_c=1.56+i0.06 [12] (the small imaginary part of the refractive index accounts for the absorption of chitin). Refractive index measurements on chitin, on the other hand, shown that chitin has substantial dispersion over the UV-vis-NIR range, in particular an increase of absorption in the NIR.

The hemispherical reflectance spectrum of the corrugated wing was calculated by the Rigorous Coupled wave Analysis (RCWA) method for normally incident light [8]. The RCWA method solves exactly Maxwell equations in laterally periodic stratified optical media and relies on Fourier (plane wave) expansions of the layer permittivity and of the electromagnetic field [8]. Its numerical implementation slightly departs from the exact analytical solution because of the necessary truncation of Fourier series. Numerical convergence of the results is improved by increasing the number of Fourier components (plane waves). In the present case, we had to use up 7×7=49 plane waves to reach satisfactory convergence [8]. The reflectance, as simulated by RCWA, was lower than 2% over the UV-visible range (Fig. 1-c), as compared to 5% average value for a flat wing (not shown), thanks to AR effect

provided by the surface corrugation [8]. Simulations performed with/without corrugation on the backside of the wing model showed that the backside corrugation helped further decreasing the reflectance at longer wavelengths (λ>700 nm) [8]. We checked that the low reflectance level was preserved when incidence angles increased up to 70°.

In the literature, various effective medium approximations are often used in order to calculate the reflectance of nipple arrays [11]. As a result, the calculation is considerably simplified since the corrugation is treated as a stack of planar homogeneous layers of gradually varying *effective* refractive indexes. The effective permittivity of each layer, $\varepsilon_{eff}=(n_{eff})^2$, can be calculated by Bruggeman's formula applied to air(ε_a=1)/chitin(ε_c) mixed medium [7]: $\varepsilon_{eff}=[g+(g^2+8\varepsilon_c)^{1/2}]/4$ with $g=(3f-1)\varepsilon_c-3f+2$ (f: air filling fraction). For an array of truncated cones separated by the distance a, the air filling fraction is $f(z)=\pi(r(z)/a)^2$, where $r(z)$ is the local radius of the cone in the layer (depicted as a yellow cylinder in Fig. 1-b). An approximation of Bruggeman's formula was used by Stavenga and coworkers, $n_{eff}=[f(n_c)^q+(1-f)]^{1/q}$ with q=2/3, as well as a simple weighting formula, $\varepsilon_{eff}=f\varepsilon_c+(1-f)$ [11]. The exact (RCWA) and approximate (effective medium) reflectance spectra are compared in Fig. 1-c. It appears that all the above mentioned effective medium approximations slightly overestimate the reflectance in the UV-visible range. In particular, the weighting formula gives the highest discrepancy. The RCWA method, unlike the effective medium methods, is able to calculate diffraction efficiencies and their corresponding contributions to the hemispherical reflectance. Here, we found that up to eight diffraction orders, in addition to the specular direction of reflection, contributed to the hemispherical reflectance in the UV range (Fig. 1-d).

3. Coloration

The male *Hoplia coerulea* beetle (Fig. 2-a) is known to exhibit blue-violet iridescence. Flat circular scales cover the upper part of the insect body (Fig. 2-b,c). The porous air/chitin multilayer (Fig. 2-d) that is buried beneath the thin envelope of the scale has been identified to be responsible for the blue coloration [13]. A photonic model involving a periodic 1D stack of dense chitin layers and mixed air/chitin effective layers (Fig. 2-d) has proven to be accurate enough in accounting for the observed reflectance spectrum and its shift with the incidence angle (i.e. iridescence) [13]. Accidently, it has been also observed that the elytra turn to emerald green upon impregnation with water [14]. This unexpected spectacular color change, which is reversible upon drying, was explained by the filling of the scale porous structure with water, a mechanism which was supported by measurements and simulations of the reflectance spectrum as function of the incidence angle [14].

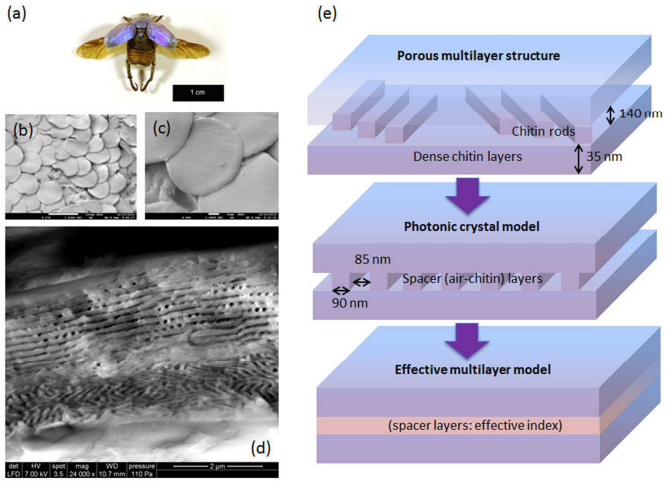

Fig. 2. (a) Photograph of male *Hoplia coerulea* beetle; (b,c) SEM images (different magnifications) of scales covering the elytron; (d) SEM image of a broken scale (cross section) revealing the thin envelope and the buried porous multilayer; (e) photonic model of the porous structure.

The hygrochromic property of *Hoplia coerulea* was further investigated through impregnation experiments with various liquids (water, methanol, ethanol, isopropanol, toluene) in order to evaluate the capacity of the porous cuticle to act as a template for developing optical sensors [9]. A droplet of 0.5 µl was deposited on an elytron (Fig. 3-a) and optical microscope images (Fig. 3-b to d) were recorded in real time in order to observe the dynamics of the color change. For all the tested liquids, the scales turn to green, one by one, but at different speeds. With water, all scales turn green after ~9 s. For some liquids other than water, evaporation took place before all scales had their color changed. Surprisingly, color changes were slower with ethanol (~70 s) than with water, in spite of the higher affinity of ethanol with bulk chitin. This counterintuitive result will be discussed later. The reflectance spectra of the elytron were also recorded in real time after droplet deposition using a fiber-optic spectrophotometer. Light was launched at normal incidence and detected in backward direction using a bifurcated optical fiber. Substantially different color change dynamics were observed according to the liquid (Fig. 3-e to g). In all cases, however, the initial color was recovered after evaporation of the liquid upon drying. Interestingly, the recovery of the blue color of the elytron upon drying was previously observed to occur by patches [14]. Here we see that patches are also found at the level of the scales.

The physicochemical properties of the liquid are expected to play a key role in the dynamics of color change, together with the composition of the chitin cuticle. For instance, among all the tested liquids, toluene is the only non-polar molecule, has the highest refractive index (n_l=1.5013) and exhibits fast evaporation. As a result, in comparison with water, less scales turned to green and they did it more slowly. The green color was also darker, due to the lower RI contrast with chitin (n_c=1.56). In general, the affinity of the liquid with chitin is likely to be influenced by molecular functional groups (alcohol, ketone, nitrile, ether…) and the strength of molecular dipole moment. On a microscopic level, it is still not clear how does the liquid infiltrate the inner porous chitin structure. The existence of a thin, apparently dense chitin envelope rules out the possibility of water infiltration through mesopores on the scale surface. The existence of micropores, which are too small to be observed on SEM images (Fig. 1-c), could explain such a rapid infiltration. In any case, *Hoplia coerulea* provides us with a quite remarkable and intriguing example of liquid-induced color changes in an apparently sealed porous structure.

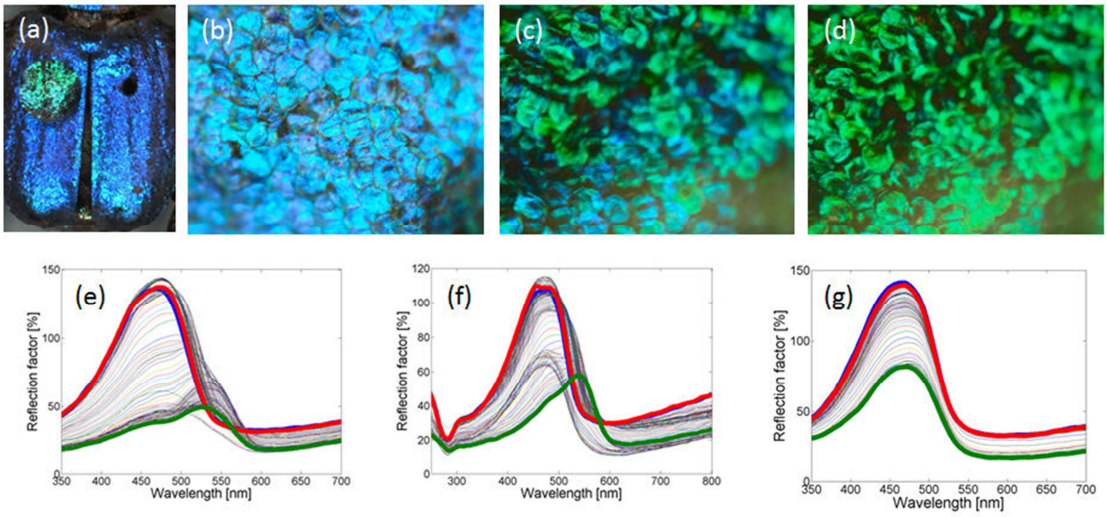

Fig. 3. (a) Macrophotograph of *Hoplia coerulea* following the deposition of a water droplet (green patch); (b-d) optical microscope images of the scales at different times following water droplet deposition (t=0s, 4.5s, 9.0s); (e-g) Real time evolution (thin curves) of the reflection factor following the deposition of water (e), ethanol (f), toluene (g) droplet - thick blue curves: in ambient conditions (before droplet deposition), thick green curves: in wet state, thick red curves: after complete drying.

4. Wettability

The transparent wings of *Cicada orni* (Fig. 4-a) exhibit nipple-like protuberances (Fig. 4-b,c) on their surface [10]. The shape of the protuberances is characterized by a cone-like base and a spherical cap which, as we will see it, provide two levels of functionality (respectively, antireflection and super-hydrophobicity). Different photonic models of the surface corrugation (Fig. 4-d) were devised in order to study the roles of the conical base and of the spherical cap in the AR property. From the comparison between measured and simulated transmittance spectra, it turned out that the spherical cap had negligible effect on AR whereas the conical base (w.r.t. cylindrical base) was essential to provide the graded refractive index profile [10]. We concluded that the AR property was essentially provided by the lower level of the nanostructure (conical base).

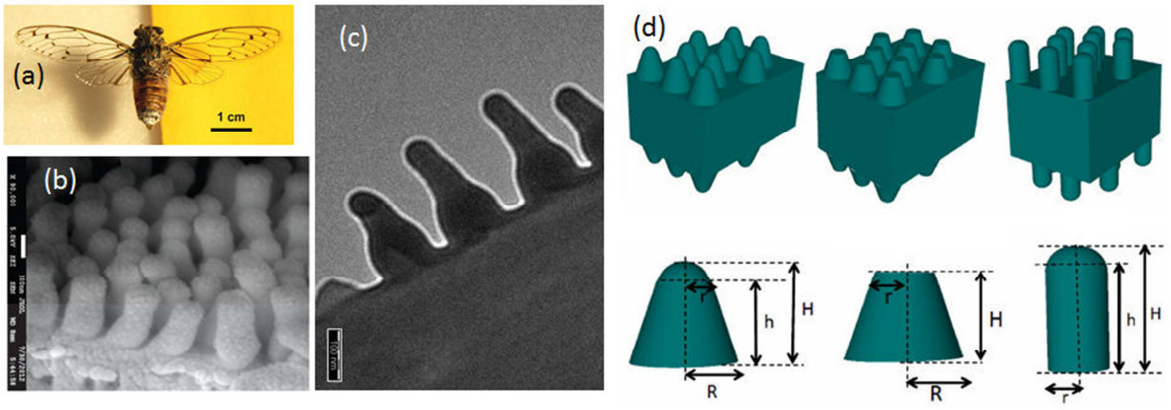

Fig. 4. (a) Photograph of *Cicadia orni* displaying transparent wings; (b) SEM image of nipple-like protuberances covering the wing surface [10]; (c) Transmission electron microscopy (TEM) image of the protuberances showing the conical bases and spherical caps; (d) photonic models (hexagonal lattice, a_0=170 nm) - left to right: capped cone, truncated cone, capped cylinder (r=40 nm, R=85 nm, H=200 nm, h=160 nm) [10].

In order to evaluate wetting properties of the wings of *Cicada orni*, measurements of the effective contact angle were performed with liquids of various surface tensions (Fig. 5-a to d). Dilution of ethanol in water enabled us to have access to liquid-air surface tensions (at 20°C) varying from γ_{LG}=72.75 mN/m to (100% water) to γ_{LG}=22.31 mN/m (100% ethanol). Contact angle for a water droplet was measured to be 146° (Fig. 5-e), very close to super-hydrophobicity (150°). This value was compared with the theoretical value predicted from the Cassie-Baxter hydrophobicity model [15]:

$$\cos\theta_{eff,CB} = n\pi r^2\left(1+\cos\theta\right)^2 - 1, \tag{1}$$

where r is the radius of the spherical cap, n=$(a_0^2\ \sqrt{3}/2)^{-1}$ is the surface coverage of the protuberances and θ is the contact angle on a flat surface. In this formula, a flat meniscus is assumed between protuberances (capped cones, Fig. 4-d). For a droplet of water on a flat chitin substrate, θ=105° [16]. According to (1), using r=40 nm and a_0=170 nm, we get θ_{eff}=151° (super-hydrophobicity), in close agreement with the measured value. Then, for each liquid, the corresponding value of θ was calculated from Young's equation [17]:

$$\cos\theta = 2\sqrt{\frac{\gamma_{SG}}{\gamma_{LG}}} - 1. \tag{2}$$

The use of this relation, which is strictly valid for non-polar liquids, is motivated by the sake of simplicity and the reasonably good fit obtained with experimentally determined contact angles (see below). More involved relations do exist [18, 19] but are difficult to track and not often used in practice. Using θ_{water} =105° (contact angle of water on a flat chitin surface) and γ_{LG}=72.75 mN/m (water-air), we deduce γ_{SG} (chitin-air) from (2). Then, by injecting the latter value into (2) and using the value of γ_{LG} for the corresponding liquid, we deduce the contact angle θ of the liquid on a flat chitin surface. The effective contact angle on hydrophilic surfaces, on the other hand, can be predicted by the Wenzel model [20], i.e. $\cos\theta_{eff}=r_0\times\cos\theta$ where is the roughness (determined from the observed morphology of the nanostructure, see [10] for details). The plot of θ_{eff} (measured on insect wing) versus θ (calculated from (2)) revealed the different wetting regimes (Fig. 5-f): hydrophobicity (Cassie-Baxter model), hydrophilicity (Wenzel model) and complete wetting. In the hydrophobic regime, the wetting property was essentially provided by the upper level of the nanostructure (spherical cap). We note that, though the theoretical curve (purple curve in Fig. 5-f) does not match perfectly with the experimental results, behaviours are similar. Differences are likely due to the fact that the flat meniscus approximation leading to equation (1) is too drastic.

Optical measurements and simulations, on one hand, and contact angle measurements and theoretical predictions, on the other hand, allowed us to speculate that *Cicadia orni* has evolved to produce two separate levels of functionality in a single nanostructure (protuberances): antireflection thanks to the conical base geometry and super-hydrophobicity thanks to the spherical cap geometry.

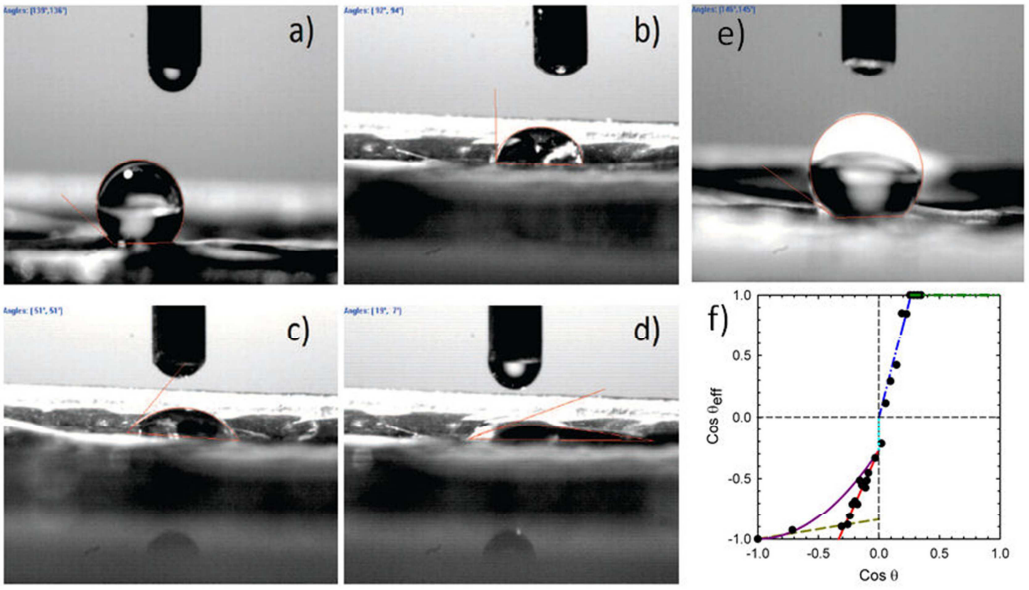

Fig. 5. (a-d) Contac angle (139°, 94°,51°, 19°) for a droplet of ethanol diluted in water (4%, 10%, 30%, 50%); (e) contact angle (146°) for a droplet of water [10]; (f) Effective contact angle θ_{eff} (measured on insect wing) as a function of contact angle θ on a flat chitin surface [10]: Wenzel model (blue curve), Cassie-Baxter model (purple curve), complete wetting (green line), guide for the eyes (red and yellowish curves). Low experimental values of $\cos\theta$=-0.7 and -1.0 were obtained using NaCl 6 M solution and Hg, respectively.

5. Conclusion

Transparency, coloration and wettability are properties of biological significance in the living world. Although they are often studied separately, there are interesting cases where these properties come together, sometimes in an intricate manner. Structural coloration and wettability were shown to be at the origin of the recently discovered hygrochromism of the male *Hoplia coerulea* beetle. Although it was unlikely that hygrochromism was related to a

biological function in the species under study, impregnation experiments with various liquids highlighted the capacity of the mesoporous cuticle to act as a template for developing optical sensors. Transparency and wettability were found to be provided by two separate levels of the same surface corrugation on the wings of *Cicadia orni*, which in this specific case are seemingly related to biological functions. This one-in-two nanostructure could be a source of inspiration for developing transparent, self-cleaned coatings such as those used in solar cell cover glasses.

Acknowledgements

This research used resources of the Electron Microscopy Service of the University of Namur (UNamur), Belgium. This Service is member of the "Plateforme Technologique Morphologie – Imagerie". This research also used resources of the "Plateforme Technologique de Calcul Intensif (PTCI)" (http://www.ptci.unamur.be) located at the University of Namur, which is supported by the Belgian National Fund for Scientific Research F.R.S.-FNRS under the convention No. 2.4520.11. The PTCI is member of the "Consortium des Équipements de Calcul Intensif (CÉCI)" (http://www.ceci-hpc.be). S.M. is supported by the F.R.S.-FNRS as Research Fellow. L. D. is supported by the Belgian Fund for Industrial and Agricultural Research (FRIA). J.-F. C. is supported by the F.R.S.-FNRS as Research Associate. M. S. is supported by Cleanoptic project (No. 1117317) of the Greenomat program of the Walloon Region (Belgium).

References

[1] K.M. Wisdom, J.A. Watson, X. Qu, F. Liu, G.S. Watson, C.-H. Chen, PNAS 110 (2013) 7992.
[2] M. Sun, A. Liang, Y. Zheng, G.S. Watson, J.A. Watson, Bioinsp. Biomim. 6 (2011) 026003.
[3] M. Rassart, J.-F. Colomer, T. Tabarrant, J. P. Vigneron, New J. Physics 10 (2008) 033014.
[4] J. H. Kim, J. H. Moon, S.-Y. Lee, J. Park, Appl. Phys. Let. 97 (2010) 103701.
[5] J. P. Vigneron, J. Pasteels, D. Windsor, Z. Vértesy, M. Rassart, T. Seldrum, J. Dumont, O. Deparis, V. Lousse, L. P. Biró, D. Ertz, V. Welch, Phys. Rev. E 76 (2007) 031907.
[6] M. Ghazzal, O. Deparis, J. De Coninck, E. Gaigneaux, J. Mat. Chem. C 1 (2013) 6202.
[7] O. Deparis, M. N. Ghazzal, P. Simonis, S. Mouchet, H. Kebaili, J. de Coninck, E. M. Gaigneaux, J. P. Vigneron Appl. Phys. Lett. 104 (2014) 023704.
[8] O. Deparis, N. Khuzayim, A. Parker, J. P. Vigneron, Phys. Rev. E 79 (2009) 041910.
[9] S. Mouchet, B.-L. Su, T. Tabarrant, S. Lucas, O. Deparis, Proc. SPIE 9127 (2014) 91270U.
[10] L. Dellieu, M. Sarrazin, P. Simonis, O. Deparis, J. P. Vigneron, J. Appl. Phys.116 (2014) 024701.
[11] D. Stavenga, S. Foletti, G. Palasantzas, K. Arikawa, Proc. R. Soc. B 273 (2006) 661–667.
[12] P. Vukusic, J. R. Sambles, C. R. Lawrence, R. J. Wootton, Proc. R. Soc. London B 266 (1999) 1403.
[13] J. P. Vigneron, J.-F. Colomer, N. Vigneron, V. Lousse, Phys. Rev. E 72 (2005) 061904.
[14] M. Rassart, P. Simonis, A. Bay, O. Deparis, J. P. Vigneron, Phys. Rev. E 80 (2009) 031910.
[15] A.B.D. Cassie, Discuss. Faraday Soc. 3 (1948) 11.
[16] M.W. Holdgate, J. Exp. Biol. 32 (1955) 591.
[17] H.-J. Butt, K. Graf, M. Kappl, Physics and Chemistry of Inter-faces, Wiley-VCH, Singapore, 2006.
[18] M. Greiveldinger, M.E.R. Shanahan, J. Coll. Inter. Sc. 215 (1999) 170-178
[19] M. Greiveldinger, M.E.R. Shanahan, C. R. Acad. Sci. Paris 11 (1999) 275-283
[20] R.N. Wenzel, Ind. Eng. Chem. 28 (1936) 988.